# Polymer−Clay Nanocomposites: A Multiscale Molecular Modeling Approach

**Giulio Scocchi,[†] Paola Posocco, Maurizio Fermeglia, and Sabrina Pricl***

*Molecular Simulation Engineering (MOSE) Laboratory, Department of Chemical, Environmental and Raw Materials Engineering (DICAMP), University of Trieste, Piazzale Europa 1, I-34127 Trieste, Italy*

*Received: November 17, 2006; In Final Form: January 7, 2007*

A hierarchical procedure bridging the gap between atomistic and mesoscopic simulation for polymer−clay nanocomposite (PCN) design is presented. The dissipative particle dynamics (DPD) is adopted as the mesoscopic simulation technique, and the interaction parameters of the mesoscopic model are estimated by mapping the corresponding energy values obtained from atomistic molecular dynamics (MD) simulations. The predicted structure of the nylon 6 PCN system considered is in excellent agreement with previous experimental and atomistic simulation results.

## Introduction

Blending molten polymer and inorganic clays can result in a class of new materials, in which nanoscale clay particles, generally layered silicates, are molecularly dispersed within the polymeric matrix. Such polymer−clay nanocomposites (or PCNs) exhibit dramatic increases in several properties, including mechanical strength and heat resistance, and a decrease in gas permeability when compared to the polymeric matrix alone.[1−7] Importantly, the improvement in these properties is achieved at very low loadings of the inorganic component, typically 1−10 wt %, thus rendering PCNs lighter in weight than any other conventionally filled polymer. These unique features make PCNs ideal materials for applications such as high barriers for food or pharmaceutical packaging to strong, heat resistant automotive components, just to name a few. Fabricating these materials in an efficient and cost-effective manner, however, poses significant synthetic challenges. To appreciate these challenges, let us discuss briefly the structure of layered silicates by considering montmorillonite (MMT) as a prime example. This inorganic clay consists of stacked silicate sheets, each approximately 200 nm long and 1 nm thick. The spacing between each sheet (or gallery) is also of the order of 1 nm, and this quantity is clearly smaller than the average radius of gyration of any conventional polymer. Therefore, entropy generally constitutes a large barrier that prevents the polymer from penetrating these galleries and becoming an intercalated material. Accordingly, there is a number of critical issues that need to be addressed in order to optimize the design and production of PCNs. Of foremost importance is the isolation of the conditions that result in a promotion of the polymer penetration into the narrow clay galleries. If, however, the sheets ultimately phase-separate from the polymer matrix, the mixture will not exhibit the improved strength, heat resistance, or barrier properties mentioned above. Accordingly, it is also essential to determine the factors that control the macroscopic phase behavior of the mixture. Finally, the properties of the PCNs commonly depend on the structure of the material; thus, it is of particular interest to establish the morphology of the final composite.

* Corresponding author. Phone: +390405583750. Fax: +39040569823. E-mail: sabrina.pricl@dicamp.unis.it.

[†] Presently at the University for Applied Sciences of Southern Switzerland (SUPSI) - Institute for Applied Computer Science and Industrial Technology (ICIMSI), Centro Galleria 2, CH-6928 Manno, Switzerland.

To date, there are few theories to pinpoint the critical parameters or to predict the thermodynamic stability of a PCN system,[8−10] forcing synthetic chemists to synthesize all possible mixtures in order to isolate the desired system. Therefore, in order to develop new materials and composites with designed new properties, it is essential for these properties to be predicted before preparation, processing, and experimental characterization. Despite the tremendous advances made in the modeling of structural, thermal, mechanical, and transport properties of materials at the macroscopic level (finite element (FE) analysis of complicated structures), there remains a tremendous uncertainty about how to predict many critical properties related to performance. The fundamental problem here is that these properties depend on the atomic level of interactions and chemistry, dealing with the electronic and atomic level of description and at a length/time scale of nanometers/nanoseconds. The material designer, however, needs answers from macroscopical modeling (the finite element paradigm) of components having scales of centimeters and milliseconds, if not larger. To substantially advance the ability to design useful high performance materials, it is then essential that we insert the chemistry into the mesoscopic (MS) and macroscopic (FE) modeling. Currently, atomistic level simulations such as molecular dynamics (MD) or Monte Carlo (MC) techniques allow one to predict the structure and properties for systems of a considerably large number of atoms and time scales of the order of microseconds. Although this can lead to many relevant results in material design, many critical issues in materials design still require time and length scales far too large for practical MD/MC simulations. Therefore, we need to develop methods treating the mesoscale in between the atomistic length and time scales of MD/MC and the macroscopic length and time scales (micrometers to millimeters and microseconds to seconds) pertaining to FE analysis. This linking through the mesoscale, in which we can describe a system microstructure, is probably the greatest challenge to developing reliable first principles methods for practical and effective material design. Indeed, only by establishing this connection from microscale to mesoscale, it is possible to build first principles methods for describing the properties of new materials and composites.

One of our major aims is to reach the domain of materials science and engineering by building from fundamental principles

10.1021/jp067649w CCC: $37.00 
Published on Web 02/10/2007

of physics and chemistry. Thus, for fundamental predictions to play a direct role in materials innovation and design, it is essential to fill the micro−meso gap. The problem here is that the current methods of coarsening the description from atomistic to mesoscale (as well as MS to FE) are not as obvious as they are from going to the quantum mechanics (QM) to the atomistic level, being strongly system-dependent and, hence, hardly generalizable. Indeed, it is quite clear that the strategy for polymers should be rather different from that adopted for metals, and again different from that conceivable for ceramic systems.

Given these concepts, it is then necessary to carry out calculations for realistic time scales fast enough to be useful in design. This requires developing techniques useful to design engineers, by incorporating the methods and results of the lower scales (e.g., MD) to mesoscale simulations. In this paper, we present a hierarchical procedure for bridging the gap between atomistic and mesoscopic simulation for polymer−clay nanocomposite (PCN) design. The dissipative particle dynamics (DPD)[11,12] is adopted as the mesoscopic simulation technique, and the interaction parameters of the mesoscopic model are estimated by mapping the corresponding energy values obtained from atomistic molecular dynamics (MD) simulations. The predicted structure of the polymer−clay nanocomposite system considered, that is, Nylon-6−Cloisite 20A, obtained from the application of the developed procedure, is in excellent agreement with previous experimental and atomistic simulation results.

## Simulation Methods and Computational Details

**DPD Theory.** In the dissipative particle dynamics simulation method,[11,12] a set of particles moves according to Newton's equation of motion and interacts dissipatively through simplified force laws. If the mass of all particles is set equal to unity, the time evolution of the positions ($\mathbf{r}_i(t)$) and momenta ($\mathbf{p}_i(t)$) is given by the well-known relationships:

$$\frac{d\mathbf{r}_i}{dt} = \mathbf{v}_i(t) \qquad \frac{d\mathbf{v}_i}{dt} = \mathbf{f}_i(t) \tag{1}$$

where the mass of each particle $i$ is set to unity and $\mathbf{r}_i$, $\mathbf{v}_i$, and $\mathbf{f}_i$ are the position vector, velocity, and total force, respectively, acting on particle $i$.

The force acting on the particles, which is pairwise additive, can be decomposed into three elements: a conservative ($\mathbf{F}_{ij}^{C}$), a dissipative ($\mathbf{F}_{ij}^{D}$), and a random ($\mathbf{F}_{ij}^{R}$) force. Accordingly, the effective force $\mathbf{f}_i$ acting on a particle $i$ is given by

$$\mathbf{f}_i = \sum_{i \neq j} (\mathbf{F}_{ij}^{C} + \mathbf{F}_{ij}^{D} + \mathbf{F}_{ij}^{R}) \tag{2}$$

where the sum extends over all particles within a given distance, $r_c$, from the $i$th particle. This distance practically constitutes the only length scale in the entire system. Therefore, it is convenient to set the cutoff radius, $r_c$, as a unit of length (i.e., $r_c = 1$), so that all lengths are measured relative to the particle radius.

The conservative force is a soft repulsion, given by

$$\mathbf{F}_{ij}^{C} = \begin{cases} a_{ij}(1 - r_{ij})\hat{\mathbf{r}}_{ij} & (r_{ij} < 1) \\ 0 & (r_{ij} \geq 1) \end{cases} \tag{3}$$

where $a_{ij}$ is the maximum repulsion between particles $i$ and $j$, $r_{ij}$ is the magnitude of the particle−particle vector $\mathbf{r}_{ij} = \mathbf{r}_i - \mathbf{r}_j$ (i.e., $r_{ij} = |\mathbf{r}_{ij}|$), and $\hat{\mathbf{r}}_{ij} = \mathbf{r}_{ij}/r_{ij}$ is the unit vector joining particles $i$ and $j$. The other two forces, $\mathbf{F}_{ij}^{D}$ and $\mathbf{F}_{ij}^{R}$, are both responsible for the conservation of the total momentum in the system and incorporate the Brownian motion into the larger length scale. They are given by the following expressions:

$$\mathbf{F}_{ij}^{D} = -\gamma\omega^{D} r_{ij}(\hat{\mathbf{r}}_{ij} \cdot \mathbf{v}_{ij})\hat{\mathbf{r}}_{ij}$$

$$\mathbf{F}_{ij}^{R} = \sigma\omega^{R} r_{ij}\theta_{ij}\hat{\mathbf{r}}_{ij} \tag{4}$$

where $\mathbf{v}_{ij} = \mathbf{v}_i - \mathbf{v}_j$, $\omega^{D}$ and $\omega^{R}$ are $r$-dependent weight functions tending to zero for $r = r_c$, and $\theta_{ij}$ is a randomly fluctuating variable with zero mean and unit variance. Español and Warren[13] have shown that one of the two weight functions in eq 4 can be chosen arbitrarily, thereby fixing the other weight function. However, the weight function and constants should obey

$$[\omega^{R}(r)]^2 = \omega^{D}(r) \qquad \sigma^2 = 2\gamma k_B T \tag{5}$$

where $k_B$ is the Boltzmann constant.

In the DPD model, individual atoms or molecules are not represented directly by the particle, but they are coarse-grained into beads. These beads represent local "fluid packages" able to move independently. Incorporation of chain molecules simply requires the addition of a harmonic spring force between the beads:

$$\mathbf{F}_{ij}^{spring} = K\mathbf{r}_{ij} \tag{6}$$

By means of this spring, the beads can interconnect to highly complex topologies. In this work, however, the calculations are performed with linear chains only.

**Model Building.** A simplified model, assuming all montmorillonite platelets to be at low volume concentration and fully dispersed in the polymer matrix in such a way that they do not interact, consists of polymer molecules interacting with both quats and the exposed silicate surface on one side of a MMT clay platelet.[14−16] The chemical structure of MMT is derived from the mineral pyrophyllite by random substitution of Al by Mg ions. The principal building elements of this mineral are 2-D arrays of aluminum−oxygen−hydroxyl octahedra sandwiched between two 2-D arrays of silicon−oxygen tetrahedra, forming a three-layered platelet. Thus, starting from relevant crystallographic coordinates,[17] we built the unit cell of pyrophyllite crystal using the *Crystal Builder* module of the *Materials Studio* molecular modeling package (v. 4.0 Accelrys, San Diego, CA). To obtain the corresponding crystal structure of MMT, some aluminum ions must be substituted by magnesium ions. In order to model a MMT with a cation exchange capacity (CEC) of approximately 92 mequiv/100 g (roughly corresponding to the CEC of one of the most commonly employed commercial products, Cloisite 20A from Southern Clay Products, Inc. (Gonzales, TX)), we first replicated the basic cell three times in the *a* direction and two times in the *b* direction (thus obtaining a supercell of dimensions 15.5 Å × 17.9 Å × 10 Å) and then substituted four Al atoms with an equal number of Mg ones. Accordingly, the resulting MMT model can be chemically described by the unit formula $(Al_{3.33}Mg_{0.67})Si_8O_{20}(OH)_4 - Na_{0.67}$). Last, the charges on the individual atoms were placed following the charge scheme proposed by Cygan et al.,[18] and this finally yielded the overall neutral MMT cell model that was used in all subsequent simulations.

The following step consisted of modeling the alkylammonium cation molecule, or quat, which was chosen to be dimethyl−dehydrogenated tallow−quaternary ammonium chloride, in accordance with the idea of modeling Cloisite 20A. After being sketched, the geometry of the molecule was optimized using the *Compass* force field (FF)[19−21] The choice of the *Compass*

FF resulted from a compromise between good accuracy and availability of force field parameters for all atom types present in the molecular model. The quat conformational search was carried out using our well-validated combined molecular mechanics/molecular dynamics simulated annealing (MDSA) protocol,[14−16,22−29] in which the relaxed molecular structure is subjected to five repeated temperature cycles using constant volume/constant temperature (NVT) MD conditions. At the end of each annealing cycle, the structure is again energy minimized, and only the structure corresponding to the minimum energy is used for further modeling. The electrostatic charges for the geometrically optimized quat molecule were finally obtained by restrained electrostatic potential fitting,[30] and electrostatic potentials were produced by single-point quantum mechanical calculations at the Hartree−Fock level with a 6-31 G* basis set. All ab initio calculations were carried out with the *DMol*$^3$ module,[31] as implemented in the *Materials Studio* modeling suite.

Finally, we modeled the polymer chains, choosing Nylon-6 as the prototype of a polymer, given the large number of studies in the literature about nanocomposites with this matrix.[32−36] In order to obtain a reasonable sampling of the polymer conformational space, we built 10 different configurations of three Nylon-6 chains at 298 K with a density of 1.12 g/cm$^3$. This was achieved by using the *Amorphous Cell* module of *Materials Studio*, which uses a version of the RIS method[37] for generating polymer chain configurations. In short, the procedure consisted of building and optimizing the polymer constitutive repeating unit (CRU) again using the *Compass* FF, which was then polymerized to a conventional degree of polymerization (DP) equal to 10. Explicit hydrogens were used in all model systems. Each polymeric structure was then relaxed and subjected to the same MDSA protocol applied to model the quat molecule. Each final chain structure was assigned atomic charges using the charge scheme proposed by Li and Goddard.[38] Moreover, we have applied the same procedure to build a Nylon-6 chain of DP = 30 to be used in the simulations of the intercalated system, as explained below.

**MD Simulations—Interaction and Binding Energies.** Resorting to atomistic MD simulations in the NVT ensemble allows the retrieval of important information on the interaction and binding energy values between the different components of a PCN system.[14−16,28,39] The technique basically consists of simulating the interface between the exfoliated organoclay and the polymer by building a cell that is "stretched" along the *c* direction (up to 150 Å); in this way, even if the model is still 3-D periodic, there are no interactions between the periodic images in the *c* direction, ultimately resulting in a pseudo 2-D periodic system,[40] from which the binding energies between all system components can be calculated. According to our procedure, we first separated the two MMT layers by 150 Å, and then, we substituted the $Na^+$ atoms of the lower MMT sheet with the quat molecules. We then copied each of the 10 Nylon-6 configurations in 10 identical cells, thus obtaining 10 different model systems. The center of mass of each polymer chain configuration was located approximately 40 Å above the center of mass of the lower MMT sheet.

The NVT simulations were performed with the *Materials Studio Discover* module, using the *Compass* FF and the charge scheme described previously. In order to reduce computational time, during each MD, both montmorillonite layers were treated as rigid bodies by fixing all cell dimensions. All other atoms in the interlayer space (except the $Na^+$ ions of the MMT upper platelet) were allowed to move without any constraint.[14−16] Each NVT simulation was run at 298 K for 500 ps, applying the Ewald summation method[41] for treating both van der Waals and electrostatic interactions. An integration time step of 1 fs and the Nosé thermostat[42] (*Q* ratio = 1) were also adopted.

For the binding energy ($E_{bind}$) calculations, we started from the concept that the total potential energy of a ternary system composed, for instance, of Nylon-6 (N6), montmorillonite (MMT), and quats (Q) ($E_{(N6-MMT-Q)}$), may be written as

$$E_{(N6-MMT-Q)} = E_{N6} + E_{MMT} + E_Q + E_{N6-MMT} + E_{MMT-Q} + E_{N6-Q} \quad (7)$$

where the first three terms represent the energy of Nylon-6, MMT, and quat (consisting of both valence and nonbonded energy terms) and the last three terms are the interaction energies between each of two component pairs (made up of nonbonded terms only). By definition, the binding energy ($E_{bind}$) is the negative of the interaction energy. To calculate the binary binding energy $E_{bind}$(N6−Q), for instance, we first created a N6−Q system deleting the MMT platelet and the $Na^+$ ions from one of the equilibrated MD trajectory frames and then calculated the potential energy of the system ($E_{N6-Q}$). Next, we deleted the quat molecules, leaving the three Nylon-6 chains alone, and thus calculated the energy of the N6 molecules ($E_{N6}$). Similarly, we deleted the three Nylon-6 molecules from the N6−Q system and calculated $E_Q$. Then, the binding energy $E_{bind}$(N6−Q) can be calculated from the following equation:

$$E_{bind}(N6-Q) = E_{N6} + E_Q - E_{N6-quat} \quad (8)$$

Similarly, the binding energies $E_{bind}$(N6−MMT) and $E_{bind}$(MMT−Q) can be computed as follows:

$$E_{bind}(N6-MMT) = E_{N6} + E_{MMT} - E_{N6-MMT} \quad (9)$$

$$E_{bind}(MMT-Q) = E_{MMT} + E_Q - E_{MMT-Q} \quad (10)$$

As the MD frame choice is concerned, we decided to calculate the system energies at 300, 350, 400, 450, and 500 ps. We considered these as representative energy values, since every energy component is well equilibrated after approximately 100 ps of simulation. All data collected have then been averaged over the 10 different model systems.

**MD Simulations—Interlayer Organic Density.** It is well-known, both from simulation[14−16,43−47] and from experimental studies,[32,34] that the presence of layered silicates in a polymer matrix causes modifications in the chain conformation next to the particle surface. In particular, considering the density of the organic species, there seems to be a tendency of the quats and polymer chains to adopt a layered conformation.[43,44] In order to investigate this behavior, we developed an original procedure to simulate quat and polymer chain intercalation into the clay galleries. For the simulations, we used the same molecular models employed in the NVT binding energy calculations described above.

Starting from the 3 × 2 MMT supercell, we removed one $Na^+$ ion and substituted it with a quat molecule, laying between the MMT sheets; we then performed a geometry optimization of the system, keeping all cell parameters fixed except for the *c* distance, and using a convergence criterion of $10^{-4}$ kcal/(mol Å). The resulting configuration was then subjected to the MDSA procedure, in order to sample as many system configurations as possible. The total simulation lasted 25 ps, with a time step of 1 fs, and consisted of five annealing cycles with a starting temperature of 298 K, a midcycle temperature of 1500 K, and

five heating ramps per cycle. The Ewald method[41] was again employed for treating the nonbonded energy components, and the Nosé thermostat[42] was chosen for temperature control. After each cycle, a molecular geometry optimization was run with the same criteria described before. Finally, the lowest potential energy conformation from the five different frames obtained as output from the described procedure was selected for further modeling.

This frame was used as an initial configuration for the insertion of the second quat molecule after removal of another $Na^+$ ion. We then applied the same procedure described above and repeated it until all four $Na^+$ atoms were substituted by quat molecules. The simulated *d*-spacing of this system was equal to 2.49 nm, which is in good agreement with the corresponding experimental values for Cloisite 20A.[48] The resulting configuration with four quats was in turn used as the initial configuration for the polymer chain insertion. To this purpose, we used the 30-monomer polymer chain built with the procedure described above and inserted into it five monomers at a time. Each time five new monomers were added, we modified the charges on the chain end atoms in order to have a zero-charge system and replaced them with their original values once the other five monomers were added and bonded to the chain end. Every time we inserted a new five-monomer set, we performed the same optimization procedure described above for the quat insertion. Accordingly, the final system was a MMT cell with four quats and a Nylon-6 chain with DP = 30, characterized by a *d*-spacing of 4.22 nm, once again in good agreement with the experimental values calculated by Fornes et al.[48] This was subjected to the last NVT annealing run, from which we selected the lowest potential energy frame from the trajectory file and used it as the starting configuration to perform a productive 300 ps NVT run, always using the *Compass* FF. Once the simulation was completed, 30 frames were extracted from the corresponding trajectory file, and on each one, we performed a concentration profile calculation of the organic species (polymer and quat) within the interlayer space.

**DPD Simulations.** In order to simulate the morphology of the organic species between the montmorillonite layers at a mesoscopic level, we used the DPD simulation tool as implemented in the *Materials Studio* modeling package. In the framework of a multiscale approach to PCN simulation, the interaction parameters needed as input for the mesoscale level DPD calculations have been obtained by a mapping procedure of the binding energy values between different species obtained from simulations at a lower (atomistic) scale.

The first step necessary for the determination of the DPD input parameters generally consists of defining the DPD bead dimensions, thus implicitly defining the characteristic length of the system ($r_c$). As illustrated in the DPD Theory section, the interaction range $r_c$ sets the basic length scale of the system; in other terms, $r_c$ can be defined as the side of a cube containing an average number of $\bar{\rho}$ beads. Therefore,

$$r_c = (\bar{\rho} V_b)^{1/3} \tag{11}$$

where $V_b$ is the volume of a bead. Thus, even in a heterogeneous system consisting of several different species, such as PCNs, a basic DPD assumption is that all bead types (each representing a single species) are of the same volume, $V_b$. Starting with the quat molecules, which consist of a strongly polar "head" and two almost apolar "tails", we considered them as being made up of two different kinds of beads. Further, in light of the above-mentioned assumption, we decided to describe each single

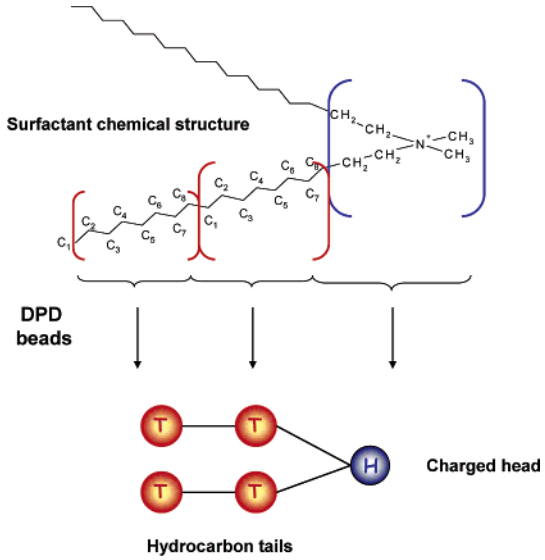


**Figure 1.** Schematic drawing of the surfactant mapping from atomistic representation to DPD beads.

alkylammonium molecule by five beads, one for the head and two for each tail, as illustrated in Figure 1.

The chosen bead volume has an average value of 130 Å$^3$, that roughly corresponds to that of a single monomer of Nylon-6, as evaluated by the Connolly algorithm.[49] The corresponding Nylon-6 chain was chosen to be 100 beads long.

Once we determined the bead size, and fixed the system density to $\rho = 3$, we could calculate the characteristic dimension of the mesoscopic system (i.e., the cutoff distance ($r_c$)) from eq 11, obtaining $r_c = 7.4$ Å. As said, this value represents the soft potential cutoff distance but is also the length of one of the unit cells in the DPD simulation box. Our DPD system was chosen to be constituted by 20 × 20 × 6 unit cells, and hence was characterized by effective dimensions of 146.1 Å × 146.1 Å × 43.8 Å. To represent the clay platelets, we made use of the available software option of including a repulsive wall in the simulation box, perpendicular to the *z*-axis at the origin. Further, we introduced a bead with no connectivity and no repulsion toward the wall, in order to fill the space between the two wall surfaces, thus representing a MMT platelet (see Figure 2).

Having set the DPD box dimensions, we proceeded by calculating the number of quat molecules that had to be inserted in order to match the CEC of the MMT used in molecular dynamics simulations. The clay surface in our atomistic molecular model has an area of approximately 277.3 Å$^2$ (i.e., 15.5 Å × 17.9 Å) and bears a charge of −2e; accordingly, two quat molecules can be placed on it. Each surface in the DPD has an area of roughly 21 351 Å$^2$ (i.e., 146.1 Å × 146.1 Å) and hence is 77 times larger than the molecular model surface and bears a charge of −154e. Accordingly, the total number of quat molecules to be inserted in our DPD box is 308 (154 for each platelet). The number of MMT beads to be inserted can in turn be calculated once the volume of the MMT platelet molecular model (2387 Å$^3$) is known. This leads to a total of 1414 MMT beads. Finally, with 7200 being the total number of beads in the box and the number of quat beads estimated to be 1540 (=308 × 5), the number of polymer beads is 4246 (=7200 − (1540 + 1414)).

After choosing the bead size, determining system dimensions and bead numbers, we used the binding energies obtained from atomistic MD simulations to calculate the values of the interaction parameters for the DPD simulation. The procedure

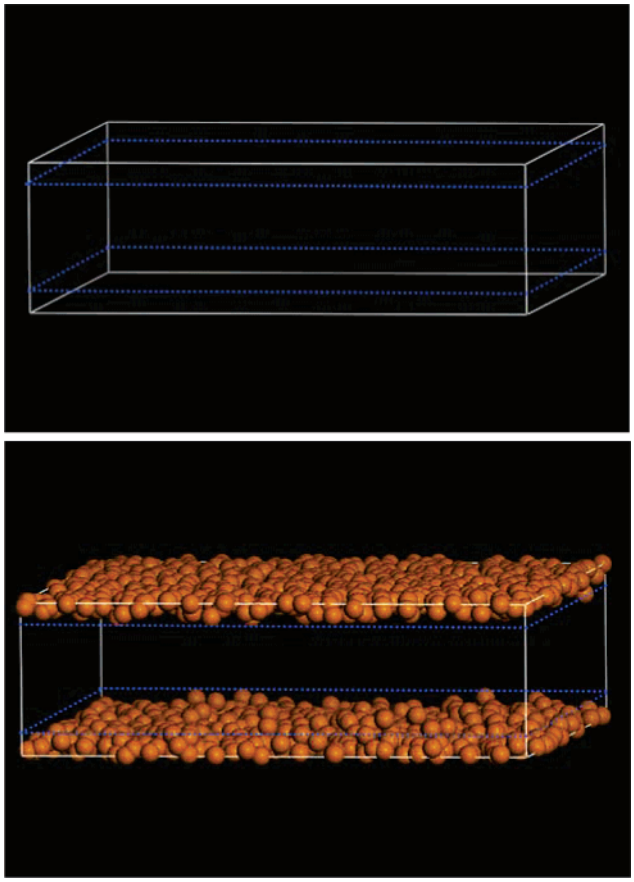

**Figure 2.** Schematic representations of the DPD repulsive wall used in this work (see text for details).

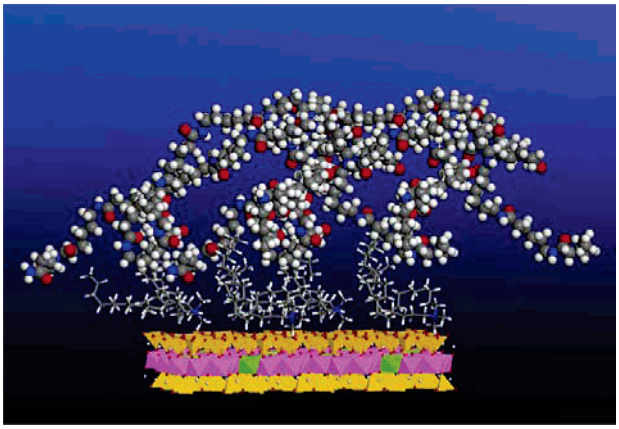

**Figure 3.** Frame extracted from the equilibrated MD trajectory at $T = 298$ K of a system made up of a MMT platelet (polyhedron style), Nylon-6 (CPK style), and quat molecules (stick style).

used to retrieve mesoscale interaction parameters from molecular dynamics binding energies is reported in detail in the Results and Discussion section, since we consider it one of the main results of this work.

## Results and Discussion

Molecular dynamics (MD) simulations were used to predict the equilibrium conformation and the interaction energy values for the Nylon-6−MMT-based nanocomposite. Figure 3 shows one snapshot taken along the corresponding equilibrated MD trajectory at $T = 298$ K as an example.

The energy monitoring reveals that all of the components of the total energy are well equilibrated after 100−150 ps (see

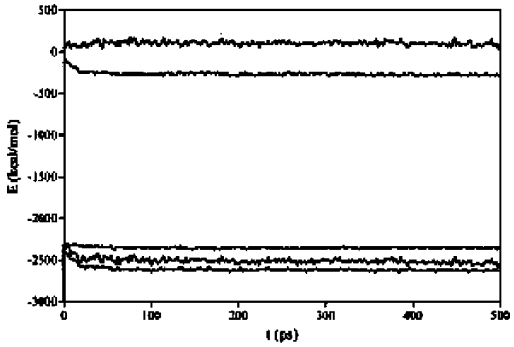


**Figure 4.** Time behavior of the potential energy components of the Nylon-6−MMT-based system during the MD simulation. Curves from top to bottom: $E_b$, valence energy; $E_{vdW}$, van der Waals energy; $E_{Coul}$, electrostatic energy; $E_{pot}$, potential energy; $E_{nb}$, total nonbonded energy.

**TABLE 1: Single Component, Binary and Ternary System Nonbonded Interaction Energies for the Nylon-6-Based Nanocomposite System Resulting from MD Trajectory Analysis (Energies Are Expressed in kcal/mol, and Standard Deviations Are Reported in Parentheses)**

| $E_{nb}$ | | |
|---|---|---|
| Nylon-6−MMT−quat | Nylon-6−quat | Nylon-6−MMT |
| −2620.95 (±14.71) | −1877.69 (±18.20) | −2103.87 (±16.35) |
| quat−MMT | Nylon-6 | quat |
| −436.78 (±11.13) | −2097.51 (±24.49) | 313.74 (±6.26) |

Figure 4). In particular, the potential energy decreases rapidly and then stabilizes around a value of −2500 kcal/mol, due to strongly favorable nonbonded interactions, as evidenced in Figure 4. The van der Waals component of the nonbonded energy diminishes as the polymer becomes closer to the clay surface, while the electrostatic contribution approaches the equilibrium value slower, because of its long-range nature.

As the simulation proceeds in time, the surfactant chains flatten onto the clay surface and cover almost the entire surface. Accordingly, the Nylon-6 chain docks on top of the quats, thereby reaching only small portions of the MMT surface. In other words, the polymer molecules tend to collapse onto the quat chains rather than directly onto the clay surface, as the quats shield the interaction between the clay and the polymer. The adsorption of the long hydrocarbon chains on the MMT layer of the clay surface finds its origin in the resulting, favorable electrostatic and van der Waals interactions.

Following our previous work,[14−16] originally based on Tanaka's approach,[39] we derived the single, binary, and ternary system interaction energies as well as the binding energies ($E_{bind}$) from the equilibrium conformation of the corresponding MD simulations. Table 1 lists the corresponding nonbonded terms ($E_{nb} = E_{vdW} + E_{Coul}$) of the calculated interaction energies; clearly, the MMT value of $E_{nb}$ is zero, as the clay framework is constrained to a fixed position during the simulation. The corresponding binding energies, calculated according to eqs 8−10, are reported in Table 2.

The values of the binding energies reported in this table are in line with our previous findings:[14−16] in fact, strong favorable interactions between clay and the surfactants exist, in harmony with the evidence from the visual inspection of the corresponding MD trajectories. The head groups of the quats are maintained in the proximity of the MMT layer by virtue of a strong electrostatic attraction, while the tails positively interact, mainly via van der Waals forces, with the clay platelet, ultimately

**TABLE 2: Binary Equilibrium Binding Energies Calculated Using eqs 2−4 for a System Made up of Three Chains of Nylon-6, Two Double-Tailed Surfactant Molecules, and a Montmorillonite Platelet (All Energies Are Expressed in kcal/mol, and Standard Deviations Are Reported in Parentheses)**

| $E_{bind}$ | | |
|---|---|---|
| Nylon-6−MMT | Nylon-6−quat | quat−MMT |
| −6.36 (±1.25) | −80.26 (±23.13) | −750.52 (±5.82) |

**TABLE 3: Equilibrium Total Nonbonded Energies ($E_{nb} = E_{vdW} + E_{Coul}$) for Nylon-6 (p), Quat Tails (t), Quat Heads (h), and a Montmorillonite Platelet (MMT) (All Energies Are Expressed in kcal/mol, and Standard Deviations Are Reported in Parentheses)**

| $E_{nb}^{H-P}$ | $E_{nb}^{H-MMT}$ | $E_{nb}^{H-T}$ | $E_{nb}^{H-H}$ | $E_{nb}^{T-P}$ | $E_{nb}^{T-MMT}$ | $E_{nb}^{T-T}$ |
|---|---|---|---|---|---|---|
| −1854.4 (±16.69) | −376.58 (±1.88) | 310.00 (±2.17) | 161.2 (±3.35) | −2185.90 (±10.90) | −116.50 (±0.301) | −15.98 (±1.74) |

covering and shielding it from the polymer. Also, the binding energy between Nylon-6 and the quats is favorable, and provides an efficient composite interface.

As anticipated above, to obtain a set of energy values which could be mapped onto mesoscale beads, we first split the quat structure into two parts: a head (h), which takes into account the quaternary nitrogen moiety, and the tails (t), which include the two long hydrocarbon chains (see Figure 1). We then calculated all equilibrium energy contributions to the interaction energies between these new "moieties" of the surfactant molecules and the remaining components of the system. The resultant total nonbonded values ($E_{nb}$) are reported in Table 3.

As expected, the MMT−quat interaction is mainly of an electrostatic nature in the case of the head groups; also for the tails, however, the Coulombic components remain favorable due to a delocalization of the nitrogen charge along the hydrocarbon chain in agreement with previous calculations.[14−16,39] The polymer−quat interaction is driven by favorable electrostatic interactions in the case of the heads and van der Waals dispersion forces for the tails, as expected.

The same Nylon-6−organoclay-based nanocomposite system was simulated in a second step at the mesoscale level using a dissipative particle dynamics (DPD) method. The simulations were conducted in a three-dimensional simulation box of 20 × 20 × 6 DPD reduced length units for a number of about 200 000 steps and a time step of 0.4.

The conservative force between two beads $i$ and $j$, as mentioned in the Simulation Methods and Computational Details section, is a soft repulsion acting along the line of the bead centers, and is given in absolute value and within the cutoff radius ($r_c$) by eq 3. The interaction DPD parameter ($a_{ij}$) has been linked to the $\chi$-parameter in a Flory−Huggins-type model by Groot and Warren,[50] or with the bead size by Maiti and McGrother.[51] In this work, we propose an alternative route, in which the interaction repulsive DPD parameters are coupled to the energy values resulting from the atomistic molecular dynamics simulations. An internal consistency is also established by comparing the density fields obtained by DPD and MD on the same system. Accordingly, the derivation of the conservative repulsion from a lower scale (i.e., atomistic) modeling constitutes a bottom-up, multiscale approach to the simulation of polymer−clay nanocomposites.

The DPD nanocomposite model contains four species of different beads: one for the polymer chain (P) and two for the quat (one for the polar head (H) and one for the apolar tail (T)). The last one is for the MMT surface (M). The most complicated step in the entire proposed ansatz is constituted by the proper mapping of the atomistic length scale to the mesoscale. To this purpose, the following combinatorial approach was used to rescale the nonbonded interaction energies listed in Table 3. The choice of using only the nonbonded interactions stems from the fact that they represent the most appropriate choice to describe the DPD conservative force ($F_c$) as defined by Groot and Warren.[50] Considering a system made up of single particles $i$ and $j$, the total energy of the system is given, in the hypothesis of neglecting the ternary contributions to interaction, by eq 12

**TABLE 4: Self and Mixed DPD Energies Rescaled from MD Simulations**

| $E_{ij}$ | P | T | H | M |
|---|---|---|---|---|
| P | −4.82 | −0.30 | −0.60 | −0.02 |
| T | −0.30 | −0.57 | 2.91 | −1.40 |
| H | −0.60 | 2.91 | 279.3 | −34.44 |
| M | −0.02 | −1.40 | −34.44 | 0 |

$$E_{system}^{tot} = n_{ii}E_{ii} + n_{jj}E_{jj} + n_{ij}E_{ij} + n_{ji}E_{ji} \tag{12}$$

where

$$n_{ii} = \frac{n_{ii}(n_{ii} - 1)}{2} \tag{13}$$

is the number of contacts between $n_i$ particles of type $i$, and

$$n_{ij} = \frac{n_i n_j}{2} \tag{14}$$

is the number of contacts between $n_i$ particles of type $i$ and $n_j$ particles of type $j$. Since the mixed energy terms ($E_{ij}$ and $E_{ji}$) and the number of contacts ($n_{ij}$ and $n_{ji}$) are the same, the expression for the total system energy, that is, eq 12, becomes

$$E_{sys}^{tot} = n_{ii}E_{ii} + n_{jj}E_{jj} + 2n_{ij}E_{ij} \tag{15}$$

The values of self-interaction energies ($E_{ii}$ and $E_{jj}$) are easily obtainable dividing the corresponding values reported in Table 3 by the appropriated number of contacts, while the value of the system total energy ($E_{sys}^{tot}$) is derived straightforwardly from the MD simulation. Accordingly, the remaining mixed energy term, $E_{ij}$, is calculated by applying eq 15. Table 4 reports all the values of the self and mixed rescaled DPD energies.

The bead−bead interaction parameter for polymer−polymer interaction was set equal to $a_{PP} = 25$ in agreement with the correct value for a density value of $\rho = 3$.[50] The value of the polymer−head interaction (i.e., $a_{PH} = 32$) was increased with respect to polymer−polymer repulsion, to describe both qualitatively and quantitatively the effect of repulsion between a neatly charged head and a substantially apolar polymeric chain. Having fixed these two parameters, their values were then associated with the corresponding values of the DPD energies rescaled from MD simulations. Thus, to $a_{PP} = 25$ corresponds a DPD rescaled energy value of −4.82, while an energy value of −0.60 is mapped to $a_{PH} = 32$ (see Table 4). All of the remaining DPD interaction parameters ($a_{ij}$) can then easily be derived following this criterion. In the case of MMT−MMT interaction, since no energy values could be extracted from the MD simulations, we set $a_{M-M} = 15$. Finally, for the pair M−H, the parameter $a_{ij}$ was not calculated using the scaling law, but we set it to a value of 5, because of its strong negative value of the rescaled energy. The final set of DPD parameters, obtained from the scaling procedure starting from atomistic MD simulation energies, is listed in Table 5.

**TABLE 5: Bead−Bead Interaction Parameters—Self and Mixed DPD Energies Rescaled from MD Simulations**

| $a_{ij}$ | P | T | H | M | W |
|---|---|---|---|---|---|
| P | 25 | 32.5 | 32 | 33 | 330 |
| T | 32.5 | 32 | 37.8 | 30.7 | 307 |
| H | 32 | 37.8 | 496.3 | 5 | 50 |
| M | 33 | 30.7 | 5 | 15 | 0 |

As anticipated above, we made use of the option available in the DPD commercial software of including a smooth wall in the simulation box perpendicular to the *z*-axis at the origin. A solid flat wall in DPD is usually constructed as an ensemble of locally freezing DPD particles.[51,52] The frozen particles behave as normal fluid particles but maintain a fixed position and velocity. Therefore, the wall interacts with each bead in the system with a potential of the same form as the bead−bead conservative force. This force is soft and short-ranged, so beads are not strictly forbidden from passing through the barrier. We introduced a bead (M) with no repulsion toward the wall, in order to fill the space between the two surfaces, and thus represent the MMT platelet. As far as the remaining beads/wall repulsive parameters are concerned, we decided to simply scale up the interaction parameters with the MMT bead by a factor of 10. In this way, we preserved the proportion of interaction energies between clay and organic species and, at the same time, we prevented the beads from crossing the wall, taking an effective flat solid surface. The values for the interaction with the wall used in the simulations are reported in the last column of Table 5.

Figure 5 illustrates the morphology results obtained from the DPD simulations. In orange color, we have MMT beads, in blue the heads of the quats, in green the tails, and in red the polymer chains.

As can be seen comparing Figures 3 and 5, a good agreement between the atomistic and mesoscale predictions is found. A fixed wall of nanoclay is obtained, by which the polar heads of the surfactant molecules are attracted to and onto which the long, apolar hydrocarbonic surfactant tails are flattened. As can be appreciated from Figure 6, the charged parts of the surfactant remain close to the MMT layers, leaving the tails to interact with the Nylon-6 chains. However, small areas are available on the clay surface for entering in contact with the polymer, thus rendering the effective binding between the components of the nanosystem almost ideal.[53]

This morphological evidence is also supported by field density distributions of the different species of beads in the simulation box obtained from the mesoscale DPD simulations (see Figure 7). From Figure 7, it appears evident that the surfactant molecules are homogeneously distributed on the layer of the inorganic filler, leaving small areas for the contact with the polymer.

The chain organization at the interfaces was also examined by calculating the contributions to the density profiles due to the polymer and surfactant chains via atomistic molecular dynamics simulations. This profile is displayed in Figure 8.

As we can see, the system organizes into three layers inside the clay gallery. This layering effect is well-known for confined liquids,[54−56] and arises mainly from solvation forces. However, the profile obtained for confined macromolecules cannot adopt the smooth and regular aspect observed for low molecular weight confined liquids[54−56] (at least when considering a simulation box of reasonable size), since the atoms have the additional constraint of being connected along chains that run across many adjacent organic layers. Anyway, Figure 8 clearly shows that the peaks have different heights and widths, depending on their location within the gallery. The highest density peaks are those closer to the clay layers; their height is indicative of the strong affinity between the adsorbed surfactant/polymer chains and the clay surface.[57,58] The adjacent peaks are lower, as a consequence of the adsorption of the first layer

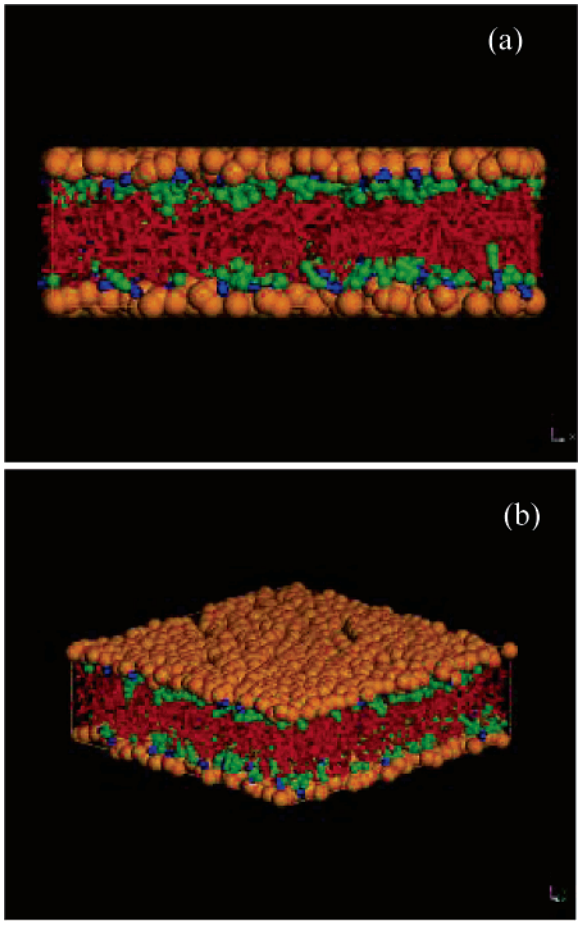


**Figure 5.** Morphology of the Nylon-6−MMT-based nanocomposite system obtained via DPD simulation: (a) perspective view; (b) frontal view. Color code: orange, MMT; blue, surfactant heads; green, surfactant tails; red, polymer.

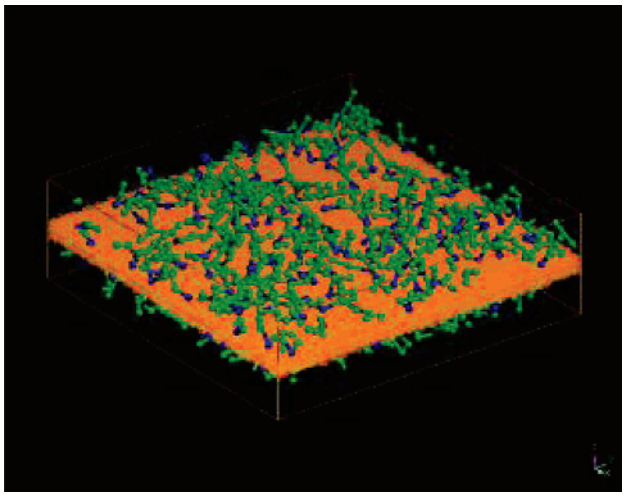

**Figure 6.** Equilibrium conformation assumed by the surfactant molecules onto the MMT layer in DPD simulations. Color code: orange, MMT; blue, surfactant heads; green, surfactant tails.

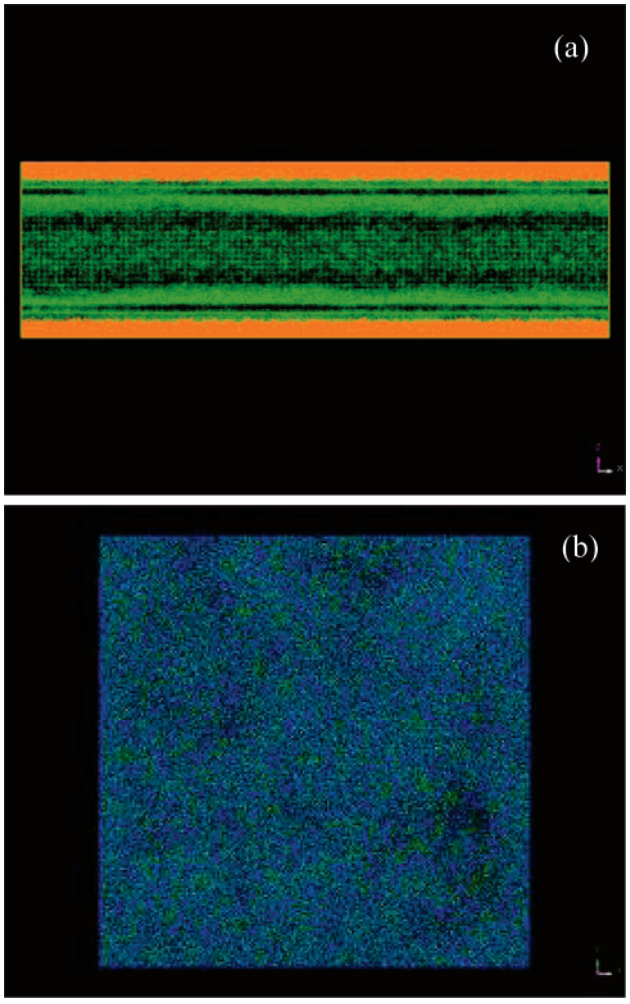


**Figure 7.** Field density distributions in the simulation cell obtained via DPD simulation. (a) Frontal view. Color code: orange, MMT; green, total organic phase (polymer and quats). (b) Top view. Color code: blue, surfactant heads; green, surfactant tails.

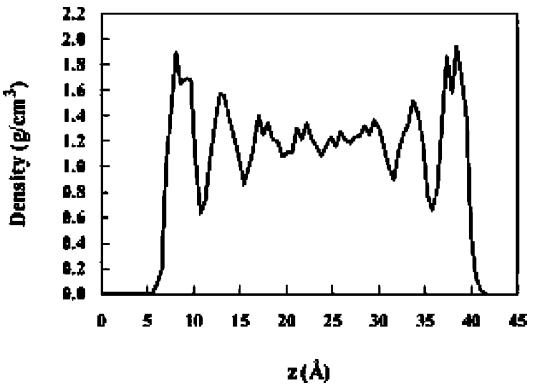


**Figure 8.** Atomistic MD density profiles of the interlayer organic phase (calculated for both polymer and surfactant chains) in the direction normal to the clay layers.

that partially shields the attractive potential of the clay surface. In the center of the gallery, practically only polymer chains are found.

The field density distribution retrieved for the mesoscale system is in agreement with the atomistic density profile; accordingly, this could be taken as a confirmation that that the atomistic model mapped onto DPD according to the proposed scaling procedure is able to reproduce a real nanocomposite polymer−clay system, thus realizing a multiscale approach to the simulation of this class of materials.

## Conclusions

There are many levels at which molecular modeling and simulation can be useful, ranging from the highly detailed ab initio quantum mechanics, through classical, atomistic molecular modeling, to process engineering modeling. These computations can significantly contribute to reduce wasted experiments, allow products and processes to be optimized, and permit large numbers of candidate materials to be screened prior to production. These techniques are currently used to obtain thermodynamic information about a pure or mixed system. Properties obtained using these microscopic descriptions assume the system to be homogeneous in composition, structure, and density, which is clearly a limitation. When a system is complex, comprising several components, eventually sparingly miscible, the PCNs being prime examples, peculiar phases with remarkable properties can be observed. These so-called mesophases comprise far too many atoms for an atomistic modeling description. Hence, coarse-grained methods are better suited to simulate such structures. One of the primary techniques for mesoscale modeling is dissipative particle dynamics, a particle-based method that uses soft spheres to represent groups of atoms and incorporates hydrodynamic behavior via a random noise, which is coupled to a pairwise dissipation. In this work, we present a hierarchical procedure for obtaining the input parameter necessary to perform polymer−clay nanocomposite DPD simulations from molecular dynamics simulations, thus bridging the gap between mesoscopic (i.e., higher length scale) and atomistic (lower length scale) modeling. The core of the proposed procedure consists of the estimation of the interaction parameters of the mesoscopic model by mapping the corresponding energy values obtained by a well-validated MD-based procedure. We applied this computational ansatz to predict the structure of a robust model system, Nylon-6−MMT PCN, and the overall results obtained are in excellent agreement with previous experimental and atomistic simulation results.

Accordingly, the simulation protocol developed in this paper may be successfully applied to other PCNs of industrial interest in different fields of application for a successful design of the material and the prediction of its final performance.

**Acknowledgment.** We acknowledge the support for the current research from the Italian Ministry of University and Scientific Research (MIUR, Rome, Italy), PRIN grant ''Theory, modeling and simulations for nanoscaled systems: applications to nanocomposites" (MF,SP). G.S. thanks the Swiss Confederation's Innovation Promotion Agency (KTI/CTI) for his Ph.D. grant through the Apolynaire project. Part of our calculations were carried out at the CSCS (Swiss National Supercomputing Center), Manno, CH, and we are grateful to Dr. Claudio Redaelli for his technical assistance. We are also indebted to Prof. Andrea Danani of SUPSI, Manno, CH, for stimulating discussions.

## References and Notes

(1) Giannelis, E. P. *Adv. Mater.* **1996**, *8*, 29.
(2) LeBaron, P. C.; Wang, Z.; Pinnavaia, T. J. *Appl. Clay Sci.* **1999**, *15*, 11.
(3) Alexandre, M.; Dubois, P. *Mater. Sci. Eng.* **2000**, *28*, 1.
(4) Schmidt, D.; Shah, D.; Giannelis, E. P. *Curr. Opin. Solid State Mater. Sci.* **2000**, *6*, 205.
(5) Pinnavaia, T. J., Beall, G. W., Eds. *Polymer-Clay Nanocomposites*; John Wiley & Sons: New York, 2000.
(6) Ray, S. S.; Okamoto, M. *Prog. Polym. Sci.* **2003**, *28*, 1539.

(7) Zeng, Q. H.; Yu, A. B.; Lu, G. Q.; Paul, D. R. *J. Nanosci. Nanotechnol.* **2005**, *5*, 1574.
(8) Balazs, A. C.; Singh, C.; Zhulina, E.; Lyatskaya, Y. *Acc. Chem. Res.* **1999**, *32*, 651.
(9) Kuznetsov, D.; Balazs, A. C. *J. Chem. Phys.* **2000**, *112*, 4365.
(10) Fornes, T. D.; Paul, D. R. *Polymer* **2003**, *44*, 4993.
(11) Hoogerbruge, P. J.; Koelman, J. M. V. A. *Europhys. Lett.* **1992**, *18*, 155.
(12) Koelman, J. M. V. A.; Hoogerbruge, P. J. *Europhys. Lett.* **1993**, *21*, 363.
(13) Español, P.; Warren, P. B. *Phys. Rev. E* **1995**, *52*, 1734.
(14) Fermeglia, M.; Ferrone, M.; Pricl, S. *Fluid Phase Equilib.* **2003**, *212*, 315.
(15) Fermeglia, M.; Ferrone, M.; Pricl, S. *Mol. Simul.* **2004**, *30*, 289.
(16) Toth, R.; Coslanich, A.; Ferrone, M.; Fermeglia, M.; Pricl, S.; Miertus, S.; Chiellini, E. *Polymer* **2004**, *45*, 8075.
(17) Tsipursky, S. I.; Drite, V. A. *Clay Miner.* **1984**, *19*, 177.
(18) Cygan, R. T.; Liang, J. J.; Kalinichev, A. G. *J. Phys. Chem. B* **2004**, *108*, 1255.
(19) Sun, H. *J. Phys. Chem. B* **1998**, *102*, 7338.
(20) Sun, H.; Ren, P.; Fried, J. R. *Comput. Theor. Polym. Sci.* **1998**, *8*, 229.
(21) Rigby, D.; Sun, H.; Eichinger, B. E. *Polym. Int.* **1998**, *44*, 311.
(22) Fermeglia, M.; Pricl, S. *AIChE J.* **1999**, *45*, 2619.
(23) Fermeglia, M.; Ferrone, M.; Pricl, S. *Bioorg. Med. Chem.* **2002**, *10*, 2471.
(24) Felluga, F.; Pitacco, G.; Valentin, E.; Coslanich, A.; Fermeglia, M.; Ferrone, M.; Pricl, S. *Tetrahedron: Asymmetry* **2003**, *14*, 3385.
(25) Pricl, S.; Fermeglia, M.; Ferrone, M.; Asquini, A. *Carbon* **2003**, *41*, 2269.
(26) Metullio, L.; Ferrone, M.; Coslanich, A.; Fuchs, S.; Fermeglia, M.; Paneni, M. S.; Pricl, S. *Biomacromolecules* **2004**, *5*, 1371.
(27) Mamolo, M. G.; Zampieri, D.; Vio, L.; Fermeglia, M.; Ferrone, M.; Pricl, S.; Scialino, G.; Banfi, E. *Bioorg. Med. Chem.* **2005**, *13*, 3797.
(28) Toth, R.; Ferrone, M.; Miertus, S.; Chiellini; Fermeglia, M.; Pricl, S. Structure and energetics of biocompatible polymer nanocomposite systems: a molecular dynamics study. *Biomacromolecules* **2006**, *7*, 1714.
(29) Fermeglia, M.; Cosoli, M.; Ferrone, M.; Piccarolo, S.; Mensitieri, G.; Pricl, S. *Polymer* **2006**, *47*, 5979.
(30) Bayly, C. I.; Cieplak, P.; Cornell, W. D.; Kollman, P. A. *J. Phys. Chem.* **1993**, *97*, 10269.
(31) Delley, B. *J. Chem. Phys.* **1990**, *92*, 508.
(32) Lincoln, D. M.; Vaia, R. A.; Whang, Z. G.; Hsiao, B. S.; Krishnamoorti, R. *Polymer* **2001**, *42*, 9975.
(33) Fornes, T. D.; Paul, D. R. *Polymer* **2003**, *44*, 3945.
(34) Maiti, P.; Okamoto, M. *Macromol. Mater. Eng.* **2003**, *288*, 400.
(35) Fornes, T. D.; Hunter, D. L.; Paul, D. R. *Macromolecules* **2004**, *37*, 1793.
(36) Chavarria, F.; Paul, R. D. *Polymer* **2004**, *45*, 8501.
(37) Theodorou, D. N.; Suter, U. W. *Macromolecules* **1985**, *18*, 1467.
(38) Li, Y.; Goddard, W. A., III. *Macromolecules* **2002**, *35*, 8440.
(39) Tanaka, G.; Goettler, L. A. *Polymer* **2002**, *43*, 541.
(40) Misra, S.; Feming, P. D., III; Mattice, W. L. *J. Comput.-Aided Mater. Des.* **1995**, *2*, 101.
(41) Ewald, P. P. *Ann. Phys.* **1921**, *64*, 253.
(42) Nosé, S. *Prog. Theor. Phys. Suppl.* **1991**, *103*, 1.
(43) Gardebien, F.; Gaudel-Siri, A.; Bredas, J.; Lazzaroni, R. *J. Phys. Chem. B* **2004**, *108*, 10678.
(44) Gardebien, F.; Gaudel-Siri, A.; Bredas, J.; Lazzaroni, R. *J. Phys. Chem. B* **2005**, *109*, 12287.
(45) Balazs, A. C. *Curr. Opin. Solid State Mater. Sci.* **2003**, *7*, 27.
(46) Sikdar, D.; Katti, D. R.; Katti, K. S. *Langmuir* **2006**, *22*, 7738.
(47) Sikdar, D.; Katti, D. R.; Katti, K. S.; Bhowmick, R. *Polymer* **2006**, *47*, 5196.
(48) Fornes, T. D.; Hunter, D. L.; Paul, D. R. *Macromolecules* **2004**, *37* (5), 1793.
(49) Connolly, M. L. *J. Am. Chem. Soc.* **1985**, *107*, 1118.
(50) Groot, R. D.; Warren, P. B. *J. Chem. Phys.* **1997**, *107*, 4423.
(51) Maiti, A.; McGrother, S. *J. Chem. Phys.* **2004**, *120*, 1594.
(52) Revenga, M.; Zúñiga, K.; Español, P.; Pagonabarraga, I. *Int. J. Mod. Phys. C* **1998**, *9*, 1319.
(53) Visser, D. C.; Hoefsloot, H. C. J.; Iedema, P. D. *J. Comput. Phys.* **2005**, *205*, 626.
(54) Israelachvili, J. N. *Intermolecular and Surface Forces*; Academic Press: San Diego, CA, 1992.
(55) Cui, S.; Cummings, P. T.; Cochran, H. D. *J. Chem. Phys.* **2001**, *114*, 7189.
(56) Fermeglia, M.; Pricl, S. *Rheol. Acta* **2001**, *40*, 104.
(57) Bitsanis, I.; Hadziioannou, G. *J. Chem. Phys.* **1990**, *92*, 3827.
(58) Klatte, S. J.; Beck, T. L. *J. Phys. Chem.* **1995**, *99*, 16024.